

---

# MACHINE-LEARNING APPLIED TO CLASSIFY FLOW-INDUCED SOUND PARAMETERS FROM SIMULATED HUMAN VOICE

---

WORKING PAPER

✉ **Florian Kraxberger**

Institute of Fundamentals and Theory in Electrical Engineering (IGTE)  
Graz University of Technology  
8010 Graz, Austria  
kraxberger@tugraz.at

✉ **Andreas Wurzinger**

Institute of Fundamentals and Theory in Electrical Engineering (IGTE)  
Graz University of Technology  
8010 Graz, Austria  
andreas.wurzinger@tugraz.at

✉ **Stefan Schoder**

Institute of Fundamentals and Theory in Electrical Engineering (IGTE)  
Graz University of Technology  
8010 Graz, Austria  
stefan.schoder@tugraz.at

July 20, 2022

## ABSTRACT

Disorders of voice production have severe effects on the quality of life of the affected individuals. A simulation approach is used to investigate the cause-effect chain in voice production showing typical characteristics of voice such as sub-glottal pressure and of functional voice disorders as glottal closure insufficiency and left-right asymmetry. Therewith, 24 different voice configurations are simulated in a parameter study using a previously published hybrid aeroacoustic simulation model. Based on these 24 simulation configurations, selected acoustic parameters (HNR, CPP, ...) at simulation evaluation points are correlated with these simulation configuration details to derive characteristic insight in the flow-induced sound generation of human phonation based on simulation results. Recently, several institutions studied experimental data, of flow and acoustic properties and correlated it with healthy and disordered voice signals. Upon this, the study is a next step towards a detailed dataset definition, the dataset is small, but the definition of relevant characteristics are precise based on the existing simulation methodology of simVoice. The small datasets are studied by correlation analysis, and a Support Vector Machine classifier with RBF kernel is used to classify the representations. With the use of Linear Discriminant Analysis the dimensions of the individual studies are visualized. This allows to draw correlations and determine the most important features evaluated from the acoustic signals in front of the mouth. The GC type can be best discriminated based on CPP and boxplot visualizations. Furthermore and using the LDA-dimensionality-reduced feature space, one can best classify subglottal pressure with 91.7% accuracy, independent of healthy or disordered voice simulation parameters.

**Keywords** Voice Signal · Voice Disorders · Aeroacoustics · Phonation

## 1 Introduction

Human phonation is the result of complex aeroacoustic phenomena such as periodical interruptions of the glottal airstream resulting in a pulsatile jet flow in the larynx, which are the main source of the human voice [1]. Using numerical models enable to analyze the cause-effect chains in the complex human phonation system. Thereby, for the driven vocal folds simulation model [2] parameters constitute the 'cause' (i.e. regular and irregular oscillation configurations, sub-glottal pressure, ...), and the simulation results the 'effect' (i.e. flow field, acoustic pressure signals, ...). According to [1], the efficiency of human phonation is mainly influenced by the vocal fold closure characteristics and the vocal fold motion properties. Thus, a high phonation efficiency is present, when the vocal folds close the glottis completely in each oscillation cycle, and when the vocal folds oscillate symmetrically as well as periodically. The phonation quality is reduced, when the glottis does not close completely or oscillates asymmetrically, resulting in a breathy or hoarse voice quality due to increased broadband components in the voice signal [3, 4, 5]. These irregularities can occur in visually healthy larynges [6, 7, 8] as well as pathological larynges [9] and their occurrence correlates with increasing patient age [10, 11].

Recently machine learning-based approaches improved the insights in voice research [12, 13, 14] and to separate healthy from disordered voices [15, 16, 17]. Using a self-organizing map based on acoustic parameters, [15] differentiated normal from disordered voices with 0.7628 accuracy. In [16] and for separation of normal, breathy, rough and hoarse voices using acoustic parameters 0.75 accuracy was achieved. Higher accuracy of 0.81, was achieved in [17] using PVG based parameters. Also, other studies showed good prediction capabilities by using acoustic measures [18, 19]. Somewhat the pure differentiation between healthy and some features associated with functional dysphonia (for instance incomplete glottis closure) is not precise since they also occur in healthy subjects [20] and some parameters are redundant [21, 22]. Regarding the broad range of possible impacts on the voice, experimental study data were enhanced with machine learning techniques to get a more profound understanding about the redundancy of which parameters best characterize functional dysphonia or other voice disorders [23].

Differently to experimental approaches (also using machine learning) and since disorders of voice production have severe effects on the quality of life, a simulation model *simVoice* [24] was developed to investigate the cause-effect chain in voice production with fully resolved data. The *simVoice* model depicts typical characteristics of voice such as sub-glottal pressure and of functional voice disorders as glottal closure insufficiency and left-right asymmetry. In total up to 80 different voice configurations were simulated. This type of simulation results in high-resolution data that can be used for machine learning techniques as input. The motivation of this paper is to demonstrate the usability of and to perform systematic investigation on the voice signal (similar to [19]). The following simulation input parameters were used: (i) four different levels of glottis closure, (ii) symmetric and asymmetric vocal fold motion of the same frequency, and (iii) three different subglottal pressures, to analyze the relation between voice signal measures such as HNR, CPP and more. Also, we have to note that this is a first study on using simulation results for machine learning in the human voice community. Furthermore, the result interpretation is limited due to the small dataset. Nevertheless, interesting conclusions can be drawn from this high-quality, high-resolution simulation dataset.

## 2 Methods

In previous works, a validated hybrid aeroacoustic model of human phonation has been established [2, 25, 26, 27], which is called *simVoice*. To reduce the computational cost of a fluid-structure-acoustic interaction model [27], a prescribed vocal fold motion model is used [28]. This model consists of a finite-volume incompressible fluid dynamics simulation, and a finite-element acoustic simulation, as documented in [29]. In [24], the model has been used to model different regular and irregular phonation characteristics, such as various degrees of insufficient glottal closure, symmetric or asymmetric vocal fold motion, and different subglottal pressures. This section is a brief introduction to the numerical model *simVoice* and the acoustic features of the simulated voice signals are defined. The aim is to discriminate against different healthy and functional-based voice disorders solely based on the evaluated acoustic features (e.g. [19]). This approach originates in voice and music research and usually uses a large number (often  $N_{\text{features}} > 20$ ) of audio features [30, 31, 32, 33]. Regarding the small dataset and the often redundant features [21], only a few features were selected for the present study are: (i) sound pressure level (SPL), (ii) Harmonics-to-Noise Ratio (HNR), (iii) Cepstral Peak Prominence (CPP), (iv) spectral slope, (v) Hammarberg Index (HBI), and (vi) Alpha Ratio (see Sec. 2.3).

### 2.1 Hybrid Aeroacoustic Simulation Setup for Human Phonation (*simVoice*)

The hybrid aeroacoustic simulation setup used to model human phonation consists of four components: (i) an incompressible computational fluid dynamics (CFD) simulation, (ii) conservative interpolation from the dense grid

of the CFD to the coarser grid of the computational acoustics (CA) simulation, (iii) computation of the aeroacoustic source term and (iv) acoustics simulation based on the Perturbed Convective Wave Equation (PCWE).

The incompressible CFD simulation is documented in [26, 28, 27] and has been performed with the software *StarCCM+*. The result thereof is the incompressible pressure  $p^{ic}$ , as described in [24], and [25] provides an in-depth analysis of the aeroacoustic source terms. The aeroacoustic source terms are furthermore filtered with the algorithm proposed in [34]. Figure 1 shows the computational domain of the CFD simulation.

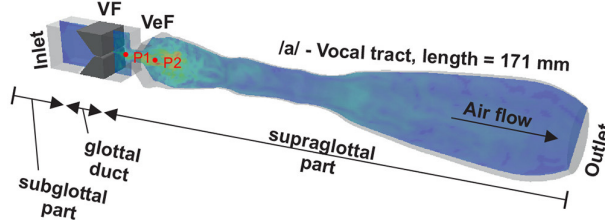


Figure 1: (color online) Computational domain of the CFD. The subglottal pressure is applied as a constant inlet pressure boundary condition [24, Fig. 2(A)].

The PCWE, as defined in [35, 2], is a wave equation regarding the acoustic scalar potential  $\psi^a$ . From the acoustic scalar potential  $\psi^a$ , the acoustic pressure  $p^a$  is evaluated.

It has been shown in [25], that the convective term can be neglected in the substantial derivative, without a significant deviation in the spectrum of the resulting acoustic pressure. The PCWE is solved using the finite-element solver *openCFS* [36]. An in-depth description of the CA simulations is available in [29, 2]. Fig. 2 shows the domain of the CA simulations consisting of the larynx, vocal tract, propagation and perfectly matched layer (PML) regions. The CA simulation domain presents an extension of the CFD simulation domain shown in Fig. 1 with a propagation and PML region. For the inlet surface, an absorbing boundary condition (ABC) was used in the CA simulations. The vocal tract and propagation regions are connected with a non-conforming (NC) interface, as described in [29]. The PML region ensures free-field wave propagation for the propagation domain [37]. The walls of the vocal tract are modeled sound-hard.

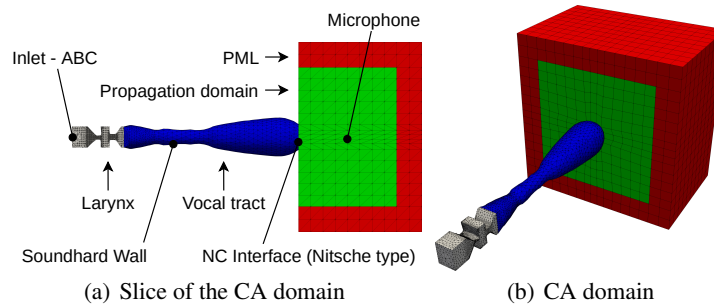


Figure 2: (color online) Computational domain of the CA simulations.

## 2.2 Phonation configurations (labels)

Voice disorders are phenomena containing complex interactions between different parts of the voice production process, such as the subglottal pressure coming from the bronchial tubes, the vocal folds (oscillating at a frequency of 148 Hz representing male voice), the false vocal folds, the vocal tract (/a/ [38]). For the present study, these interacting elements and regular (subglottal pressure) and irregular characteristics (asymmetry and insufficiency) thereof are abstracted in terms of certain functions of the voice production process (see [24]). Thus, periodic symmetric and asymmetric oscillation characteristics, different grades of glottis insufficiency, in combination with varying subglottal pressure have been simulated as described in [24, 39]. The simulation results of the acoustic pressure signal in front of the vocal tract (the mouth), are used for the later computations of the acoustic features.

**Subglottal Pressure** The presence of a pressure difference between the subglottal and supraglottal regions drives the glottal airstream. The inability to build up such a pressure can be one reason for a dysphonic voice, e.g. caused by

muscle tension disorders, as reported in [40, 41]. The simulation cases include the subglottal pressures as follows

$$P_{\text{inlet}} \in \{385, 775, 1500\} \text{ Pa.} \quad (1)$$

Where, 775 Pa represents normal subglottal pressure and the other low or high, respectively.

**Glottal Closure Type** The vocal folds can have varying degrees of glottal insufficiency, which occur when the vocal folds do not close completely in each cycle. According to [42, 43], this irregularity occurs for many voice pathologies. As a consequence, concerned patients report, that a higher effort is necessary for phonation [44]. The glottal closure (GC) type determines the amount of glottal insufficiency.  $o_{\text{initial}}$  is defined as the percentage of the vocal folds lengths which does not close. The simulation model employs initial glottal openings of

$$o_{\text{initial}} \in \{0(\text{GC1}), 40, 70, 100(\text{GC4})\} \%, \quad (2)$$

which are called GC1 (complete glottal closure), GC2 (60% of the vocal folds lengths close), GC3 (30% of the vocal folds lengths close), and GC4 (no contact of vocal folds during oscillations), respectively [24]. The different GC types are based on high-speed videos from experiments with excised larynges and are motivated by clinical observations [45, 46, 27]. A detailed description as well as visualizations of the different symmetry cases are available in Fig. 5.5 [47].

**Vocal Fold Motion Symmetry** In regular phonation, the left and right vocal fold oscillate symmetrically. However, in the case of laryngeal unilateral paresis or unbalanced muscle tension, the vocal folds oscillate asymmetrically [48, 49]. Therefore, the proposed simulation model features two cases of vocal fold motion symmetry. In the symmetric case, both vocal folds have the same amplitude in their motion. In the asymmetric case, one vocal fold oscillates with 50% of the amplitude of the other vocal fold. Both symmetry cases are depicted in Fig. 3.

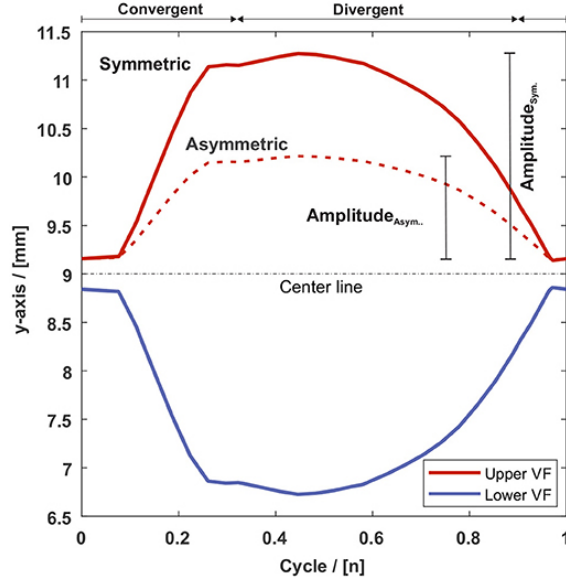


Figure 3: (color online) Exemplary vocal fold motion of GC1 for the symmetric and asymmetric case along the y-axis (medial-lateral direction) for the center point on the medial plane of the VF surface [24, Fig. 4].

In Tab. 1, the simulation parameters are summarized. A total of 24 different functional-based voice disorders have been simulated.

Table 1: Simulation parameters of functional-based voice disorders as defined in [24].

Parameter	#	Values
Subglottal Pressure	3	$P_{\text{inlet}} \in \{385, 775, 1500\} \text{ Pa}$
Glottal Closure Type	4	$o_{\text{initial}} \in \{0, 40, 70, 100\} \%$
Vocal Fold Motion Symmetry	2	asymmetric or symmetric
	24	configurations total

### 2.3 Acoustic Feature Definitions

The acoustic pressure signal results of the *simVoice* model are recorded at an evaluation point (so-called 'microphone'), as depicted in Fig. 2 (a). The recorded signal is time discrete acoustic pressure  $p[n]$  with  $n$  being the time index [50] sampled at  $T_s = 1/f_s = 13.6 \mu\text{s}$  [2, 24]. With those audio signals (one resolved signal for each of the 24 simulation configurations), we compute certain *acoustic features* for the analysis. Thus, we aim to analyze the flow-induced sound generation of health and of functional-based voice disorders by using the evaluated features only.

**Sound Pressure Level** The SPL  $L_p$  of an acoustic pressure signal  $p[n]$  is computed as follows,

$$L_p = 20 \cdot \log_{10} \frac{\tilde{p}}{p_{\text{ref}}^a} \quad \text{with} \quad p_{\text{ref}}^a = 20 \mu\text{Pa}$$

$$\tilde{p} = \sqrt{\frac{1}{N} \sum_{n=1}^N (p[n])^2}. \quad (3)$$

Thereby,  $N$  is the number of time steps of  $p[n]$ . Consequently,  $\tilde{p}$  denotes the root-mean-square of the acoustic pressure signal. The subglottal pressure is expected to have a significant influence on the sound pressure level (SPL) magnitude of the acoustic signal. Since a higher subglottal pressure (driving force of the phonation) will certainly exhibit a stronger voice at the same vocal efficiency.

**Harmonics-to-Noise Ratio** Harmonics-to-Noise ratio (HNR) provides a measure for the degree of hoarseness [51], and has since been used, among others, to identify voice disorders [52] and voice quality [53, 54]. Thus, in the present study HNR is used with the aim of contributing to the identification and analysis of glottis closure type, the asymmetry and their combinations defined in Sec. 2.2. The idea is to use the HNR to be a measure of an increasing amount of turbulent structures and decreasing tonal contribution during the whole oscillation cycles for only partly closing vocal folds. HNR is defined as the energy ratio between the harmonic signal component to the noise-like signal component in dB. The splitting of harmonic and noise-like components is performed via the auto-correlation function (ACF), as described in [31, pp. 77–78]. The ACF  $r_p(\tau)$  of a pressure signal  $p[n]$  is calculated with

$$r_p(\tau) = \sum_{n=0}^{N-1} p[n]p[n+\tau], \quad (4)$$

where  $\tau$  is the independent lag variable. Therewith, the HNR can be computed with [31, Eq. (2.234)], such that

$$\text{HNR}_{\text{dB, Eyben}} = 10 \log_{10} \frac{\max\{r_p(\tau)\}}{r_p(0) - \max\{r_p(\tau)\}}, \quad (5)$$

under the assumption that (i) the noise is additive, (ii) it is uncorrelated with the signal and (iii) the noise is uncorrelated to itself (i.e. it is white noise). To be robust against deviations from the assumptions in the simulated signal, a margin of  $k_{\text{marg}} = 300$  lag bins is introduced, which corresponds to a lag of  $\tau_{\text{marg}} = k_{\text{marg}}/f_s = 4.08$  ms. Therewith, the HNR  $h$  is calculated as follows:

$$\text{HNR}_{\text{dB}} = h = 10 \log_{10} \frac{\max_{\tau_{\text{marg}}}^{\tau_{\text{max}}} \{r_p(\tau)\}}{r_p(0) - \max_{\tau_{\text{marg}}}^{\tau_{\text{max}}} \{r_p(\tau)\}}, \quad (6)$$

where  $\tau_{\text{max}}$  is the maximum possible lag time (i.e. the time corresponding to the highest lag index).

**Cepstral Peak Prominence** The harmonic structures occurring in the voice spectrum map to peaks in the cepstral domain, as introduced in [55]. Healthy voice shows, that the harmonic parts dominate the spectrum, and thus it is expected that the corresponding peak in the cepstral domain is prominent compared to non-harmonic parts of the cepstrum. Hence, Cepstral Peak Prominence (CPP) measures the prominence of the peak in the cepstral domain and therefore the prominence of harmonic structures in the spectrum compared to non-harmonic parts. Therewith, we aim to discriminate simulation parameters which affect the harmonic structure of the voice signal, e.g. by an incomplete glottis closure. The CPP is computed as follows [56, 57]: Given a pressure signal  $p[n]$ , a power spectral density (PSD) estimate  $\tilde{p}[k]$  is computed using Welch's method [58] such that

$$\tilde{p}[k] = \sqrt{\mathcal{F}_{n \rightarrow k}\{p[n]\}[k]}$$

$$\tilde{p}_{\text{dB}}[k] = 20 \cdot \log_{10} \frac{\tilde{p}[k]}{p_0} \quad \text{with} \quad p_0 = 20 \mu\text{Pa}, \quad (7)$$

where  $\mathcal{F}_{n \rightarrow k}\{p[n]\}[k]$  denotes the PSD based on the  $N$ -point discrete Fourier transform (DFT) [50]. In accordance to [55], the cepstrum  $c_{\tilde{p}}[k]$  is computed such that

$$c_{\tilde{p}, \text{dB}}[q] = 10 \cdot \log_{10} |\mathcal{F}_{k \rightarrow q}\{\tilde{p}_{\text{dB}}[k]\}[q]|^2. \quad (8)$$

The independent variable of the cepstrum is called *quefrency* and has the dimension of *time* [55]. The CPP  $c$  is evaluated as follows [56, 57]: For quefrencies larger than 1 ms, a linear regression line is fitted to the cepstrum. The CPP is the difference between the peak amplitude of the cepstral maximum and the linear regression line evaluated at the quefrency of the cepstral maximum. Thus, it represents how far the cepstral peak emerges from the cepstral "background noise". This can be interpreted as the prominence of harmonics in the signal compared to non-harmonic signal portions. In [46, 59], it was used together with other features as a measure for vocal effort and to disambiguate different voice disorders. In [60, 61, 62], CPP and HNR are used to compute the so-called *Acoustic Voice Quality Index* together with shimmer and spectral slope and tilt. Furthermore, CPP and cepstrum-based features are used as fundamental measures in speech sciences [63, 64, 65].

**Spectral Slope** The spectral slope is a measure of energy distribution across the spectrum and is used in [66, 67] to distinguish voice qualities. If the glottal airstream is interrupted off completely in each vocal fold oscillation cycle, we expect effects on the energy distribution in the resulting acoustic signal. Thus, this feature is used to determine if high frequencies (which we expect to increase due to incomplete glottis closures) dominate lower frequencies, such that the general spectral trend represented by the spectral slope is influenced. In [31], spectral slope<sup>1</sup> is defined as the result of a linear regression operation on the whole spectrum  $\tilde{p}[k]$ . Thereby, a line  $\hat{y} = ax + b$  is fitted to the spectrum  $\tilde{p}[k] = \sqrt{\mathcal{F}_{n \rightarrow k}\{p[n]\}[k]}$ , such that the mean-squared error between the line and the original spectrum is minimized (*minimum mean-squared error* condition). The parameter of interest is  $a$ , which is the *slope* of the linear regression result. A formula for  $a$  is provided by [31], such that

$$a = \frac{N\Sigma_{xy} - \Sigma_x\Sigma_y}{N\Sigma_{x^2} - \Sigma_x^2}, \quad (9)$$

where  $N$  is the number of DFT frequency bins and  $\Sigma_{xy}$ ,  $\Sigma_x$ ,  $\Sigma_y$  and  $\Sigma_{x^2}$  are defined as follows

$$\begin{aligned} \Sigma_x &= \sum_{i=0}^{N-1} f(k_i), & \Sigma_y &= \sum_{i=0}^{N-1} p[i], \\ \Sigma_{x^2} &= \sum_{i=0}^{N-1} f(k_i)^2, & \Sigma_{xy} &= \sum_{i=0}^{N-1} f(k_i)p[i], \end{aligned} \quad (10)$$

where  $f(k)$  is the frequency in Hz associated with the frequency bin  $k$ . By exploiting the equidistant frequency scale used in the DFT, simplifications arise [31], such that

$$\Sigma_x = \frac{1}{2}N(N-1) \quad \text{and} \quad \Sigma_{x^2} = \frac{1}{6}N(N-1)(2N-1). \quad (11)$$

**Hammarberg Index and Alpha Ratio** Hammarberg Index (HBI) and Alpha Ratio are measures of the energy distribution across the spectrum. Similar to spectral slope, also these features are introduced aiming to discriminate simulation parameters which influence the glottis closure, i.e. GC type and glottis symmetry. HBI  $\eta$  as defined in [69] is the ratio of the most prominent energy peak in the range of 0 kHz–2 kHz to the most prominent energy peak in the region 2 kHz–5 kHz. It is calculated according to [31, p. 38], such that

$$\eta = \frac{\max_{k=1}^{k_{\text{pivot}}} \{\tilde{p}[k]\}}{\max_{k=k_{\text{pivot}}+1}^{k_{\text{max}}} \{\tilde{p}[k]\}}, \quad (12)$$

where the pivot frequency bin  $k_{\text{pivot}}$  is the highest spectral bin for which  $f \leq 2$  kHz, and  $k_{\text{max}}$  is the highest spectral bin for which  $f \leq 5$  kHz.

The alpha ratio is similar to the HBI described above, but instead of computing the ratio between energy peaks, the energy sum in the frequency bands is considered, as introduced in [70]. Using the frequency bands 50 Hz–1 kHz and 1 kHz–5 kHz, the alpha ratio  $\rho_\alpha$  can be computed according to [31, pp. 38–39], such that

$$\rho_\alpha = \frac{\sum_{k=k_{\text{start}}}^{k_{\text{pivot}}} \tilde{p}[k]}{\sum_{k=k_{\text{pivot}}+1}^{k_{\text{max}}} \tilde{p}[k]}, \quad (13)$$

<sup>1</sup>As shown in [68], the terms "spectral slope" and "spectral tilt" are used interchangeably in the literature, thus, for spectral slope, the definition of [31, pp. 35] is used.

where the  $k_{\text{start}}$  is the lowest spectral bin for which  $f \geq 50$  Hz,  $k_{\text{pivot}}$  is the highest spectral bin for which  $f \leq 1$  kHz, and  $k_{\text{max}}$  is the highest spectral bin for which  $f \leq 5$  kHz.

**Low-Pass Filtering** The acoustic pressure signals from the simVoice model is filtered by low-pass filter. Before the computation of all features a filter with 5 kHz cut-off frequency is used. This is due to the upper frequency limit of the simulation setup [2, 34]. In addition, and before computing CPP, HNR and spectral slope, we use a filter of 2 kHz cut-off frequency targeting only the lowest two formants [38]. The features based on both filtering strategies in total amount to 9 evaluated acoustic features per configuration  $i$ . The evaluated features for the  $i$ -th configuration ( $i = 1, \dots, 24$ ) are denoted as a vector  $\mathbf{F}^{(i)}$ , such that

$$\mathbf{F}^{(i)} = \left[ L_{P,5 \text{ kHz}}^{(i)} \quad h_{5 \text{ kHz}}^{(i)} \quad h_{2 \text{ kHz}}^{(i)} \quad c_{5 \text{ kHz}}^{(i)} \quad c_{2 \text{ kHz}}^{(i)} \quad a_{5 \text{ kHz}}^{(i)} \quad a_{2 \text{ kHz}}^{(i)} \quad \eta_{5 \text{ kHz}}^{(i)} \quad \rho_{\alpha,5 \text{ kHz}}^{(i)} \right]^T, \quad (14)$$

where  $L_P^{(i)}$  is SPL,  $h^{(i)}$  is HNR,  $c^{(i)}$  is CPP,  $a^{(i)}$  is spectral slope,  $\eta^{(i)}$  is HBI,  $\rho_\alpha^{(i)}$  is the alpha ratio, and the subscript indicates the low-pass filter's cut-off frequency.

## 2.4 Data Labeling, Dimensionality Reduction and Classification

We interpret different functional-based voice disorders as *labels* in a machine learning sense. Thus, each of the 24 configurations defined in Sec. 2.2 is labeled with one value of each of the following label sets. For the  $i$ -th configuration, this yields labels from the following label sets:

$$\begin{aligned} \ell_{\text{subglottPress}}^{(i)} &\in \{385, 775, 1500\} \\ \ell_{\text{GC}}^{(i)} &\in \{1, 2, 3, 4\} \\ \ell_{\text{sym}}^{(i)} &\in \{0, 1\}. \end{aligned} \quad (15)$$

Thus, the label  $\mathbf{L}^{(i)}$  of the  $i$ -th simulation configuration is formed as a vector

$$\mathbf{L}^{(i)} = \left[ \ell_{\text{subglottPress}}^{(i)} \quad \ell_{\text{GC}}^{(i)} \quad \ell_{\text{sym}}^{(i)} \right]^T \quad (16)$$

For example, considering the configuration with 385 Pa subglottal pressure, GC1 and asymmetric VF motion, the label vector would be  $\mathbf{L}^{(1)} = [385 \quad 1 \quad 0]^T$ . To form classes, different oscillation patterns and subglottal pressure are considered individually. Thereby, all evaluated feature vectors  $\mathbf{F}^{(i)}$  are considered to be of a certain class, if *one* element of the feature vector  $\mathbf{L}^{(i)}$  is identical. The other elements of the feature vector are discarded. For example, the class GC1 contains all data samples  $\mathbf{F}^{(i)}$ , for which  $\mathbf{L}^{(i)} = \left[ \ell_{\text{subglottPress}}^{(i)} \quad 1 \quad \ell_{\text{sym}}^{(i)} \right]^T$ , regardless of the values of  $\ell_{\text{subglottPress}}^{(i)}$  and  $\ell_{\text{sym}}^{(i)}$ . The features, as defined in Sec. 2.3, span a 9-dimensional feature space. For dimension reduction and visualization, a two-fold approach is used, consisting of (i) Linear Discriminant Analysis (LDA), see Sec. 4.1.4 of [71] and (ii) upon the results of the LDA a classification with Support Vector Machines (SVMs), see Sec. 7.1.3 of [71]. LDA is used to project the data points  $\mathbf{F}^{(i)}$  from the original feature space into a two-dimensional feature space, with the goal to maximize the distance between different classes while minimizing the covariance within each class. The results of the LDA are transformed data points  $\mathbf{F}_{\text{tf}}^{(i)}$  for which  $\dim(\mathbf{F}_{\text{tf}}^{(i)}) = 2$  for the LDA with respect to GC type (only using the first two major components for visualization) and subglottal pressure, and  $\dim(\mathbf{F}_{\text{tf}}^{(i)}) = 1$  for the LDA with respect to symmetry property. In Fig. 4, the weights of the LDA transformation are depicted.

Thereafter, the labeled data is used to train an SVM classifier with radial basis function-kernels and a one-versus-rest classification. The SVM implementation in the Python library *sklearn* has been used for this task [72]. To quantify the generalization ability of the SVM classifier, 5-fold stratified cross-validation was used [71]. The mean scores of the cross-validation data sets are shown in Tab.???. Thereafter, the whole data set was used to train the SVM classifier to classify mesh grid points to visualize the class boundaries. Based on the small number of data, the cross-validation procedure leads to stratified results but should be considered in the future with increasing amount of data.

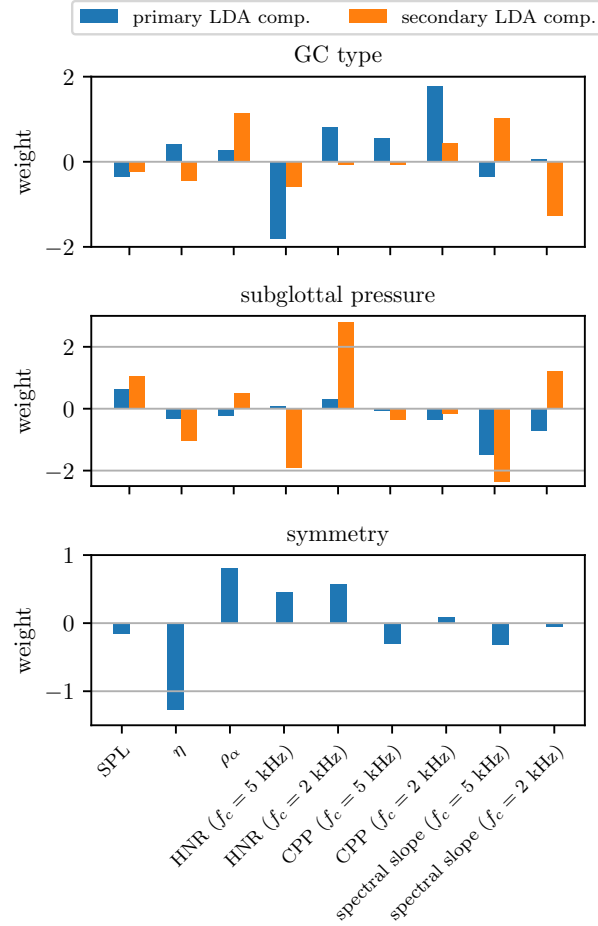


Figure 4: Feature weights for dimension reduction.

### 3 Results

First, we study Pearson’s correlation between the individual acoustic features and display it as a correlation map. In Fig. 5, the correlation map is shown for configurations evaluated from acoustic pressure at the evaluation position as depicted in Fig. 2 (a).

From Fig. 5 it is visible, that for HNR, CPP and spectral slope, which have been evaluated following a 2 kHz LP-filter provide stronger correlations than those evaluated with a 5 kHz LP-filter. Furthermore, it is visible that spectral slope does not correlate significantly with any of the modeled phonation characteristics, i.e. symmetry, GC type, and subglottal pressure. Based on the small dataset, the significance of the individual correlation based on the autocorrelation is not giving a full picture. Therefore, we continue studying the data with boxplots to get a more detailed understanding of a significant difference of the data points.



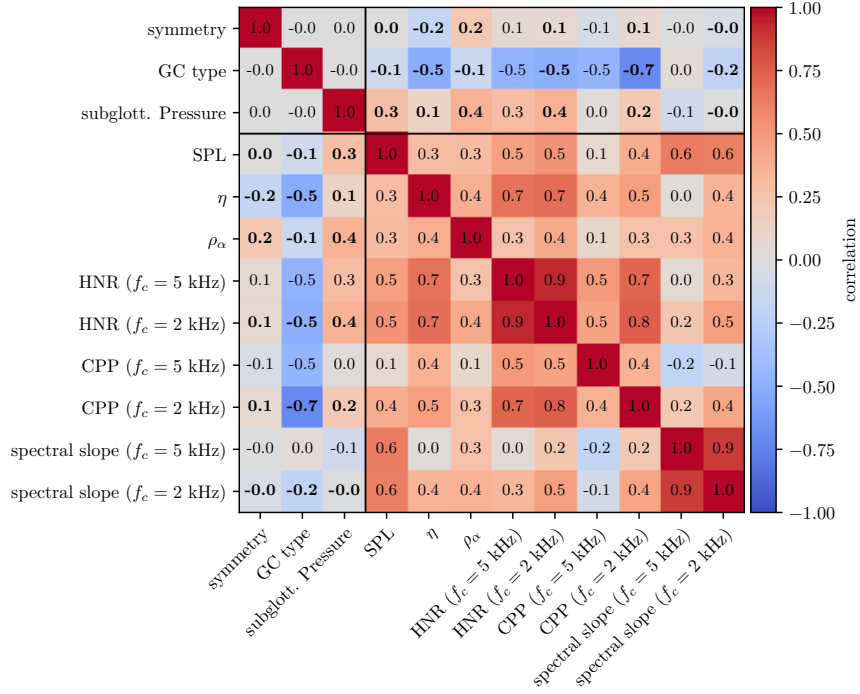


Figure 5: (color online) Correlation map between features and parameters for signals (acoustic pressure at the microphone position). The fields are colored according to the correlation value of the respective parameter combination (i.e. the number in each field). The numbers in bold highlight cause-effect-combinations which are further investigated using boxplot diagrams. The thick black lines are separating simulation parameters from evaluated features.

### 3.1 Boxplot Visualizations

In the following, boxplot diagrams are shown, which visualize the distributions of the evaluated features. Thereby, manually selected 6 features ( $L_{P,5\text{ kHz}}^{(i)}$ ,  $h_{2\text{ kHz}}^{(i)}$ ,  $c_{2\text{ kHz}}^{(i)}$ ,  $a_{2\text{ kHz}}^{(i)}$ ,  $\eta_{5\text{ kHz}}^{(i)}$ ,  $\rho_{\alpha,5\text{ kHz}}^{(i)}$ ) are used because the correlation diagram in Fig. 5 already showed, which features provide better correlations with respect to the simulation parameters. From the boxplot diagrams, we can learn, how individual features vary across different simulation parameters. They provide an insight on possible parameter groups which cannot be discriminated using individual features, but might be discriminable using a combination of features, e.g. by means of an LDA/SVM approach.

**Boxplots for Glottal Closure Type** In Fig. 6, the boxplot diagrams for the simulation parameter *glottal closure type* are depicted for the acoustic pressure evaluated at the microphone position. From Fig. 6 (A), (B), and (C), we see a general trend of decreasing CPP and HNR values with increasing initial glottal openings. A significant trend is visible for CPP evaluated with the low-pass filter at  $f_c = 2$  kHz, as shown in Fig. 6 (B).

**Boxplots for Symmetry** In Fig. 7, the boxplot diagrams for the simulation parameter *symmetry* are depicted for the acoustic pressure evaluated at the microphone position. It is shown, that no significant discrimination of glottal symmetry is possible based on the evaluated features. This is also supported by near-zero correlation values for the symmetry property depicted in Fig. 5. This non-observable difference might be due to the inhomogeneous composition of the data.

**Boxplots for Subglottal Pressure** In Fig. 8, the boxplot diagrams for the simulation parameter *subglottal pressure* are depicted for the acoustic pressure evaluated at the microphone position. A discrimination between the subglottal pressures 385 Pa and {775 Pa, 1500 Pa} is possible using HNR, SPL, Alpha Ratio  $\rho_\alpha$ , and HBI  $\eta$ , as depicted in Fig. 8 (C), (D), (E), and (F), respectively. Spectral slope allows distinguishing configurations with 775 Pa from {385 Pa, 1500 Pa}, as it can be seen from Fig. 8 (A).

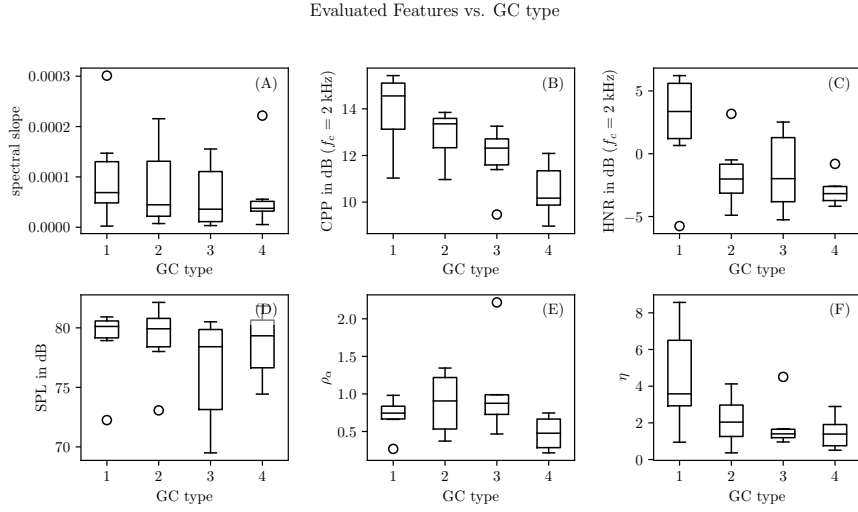


Figure 6: Boxplot diagrams of the features spectral slope  $a$ , CPP  $c_{2\text{kHz}}$ , HNR  $h_{2\text{kHz}}$ , SPL  $L_{P,5\text{kHz}}$ , alpha ratio  $\rho_\alpha$ , and HBI  $\eta$  as a function of glottal closure type for acoustic pressure signals at the microphone position.

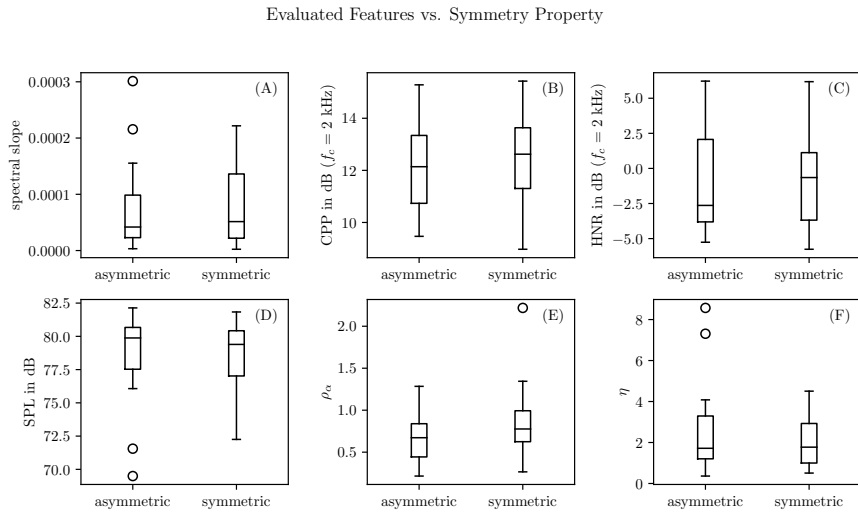


Figure 7: Boxplot diagrams of the features spectral slope  $a_{2\text{kHz}}$ , CPP  $c_{2\text{kHz}}$ , HNR  $h_{2\text{kHz}}$ , SPL  $L_{P,5\text{kHz}}$ , alpha ratio  $\rho_\alpha$ , and HBI  $\eta$  as a function of VF motion symmetry for acoustic pressure signals at the microphone position.

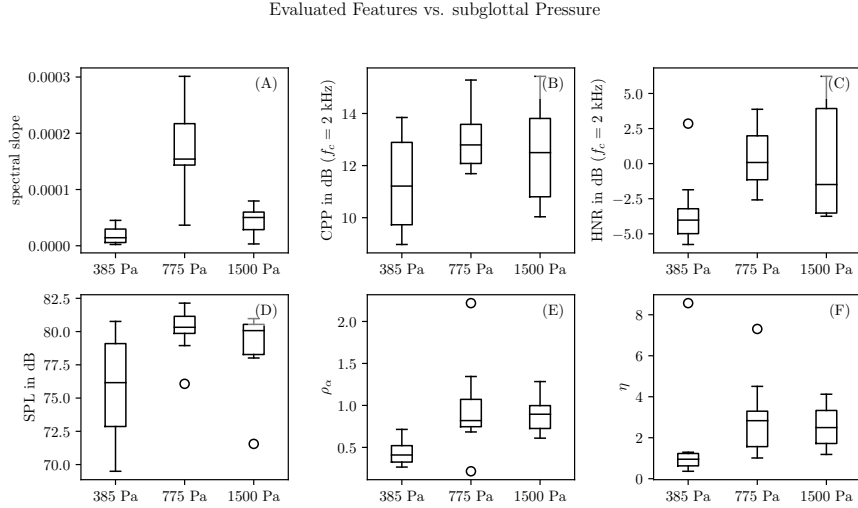


Figure 8: Boxplot diagrams of the features spectral slope  $a$ , CPP  $c_{2 \text{ kHz}}$ , HNR  $h_{2 \text{ kHz}}$ , SPL  $L_{P,5 \text{ kHz}}$ , alpha ratio  $\rho_\alpha$ , and HBI  $\eta$  as a function of subglottal pressure for acoustic pressure signals at the microphone position.

### 3.1.1 Intermediate conclusions boxplots

From the boxplot diagrams, statements regarding the significance of the features' discrimination ability can be drawn. A good discriminative ability is provided by using CPP or HNR to discriminate the GC type. The decreasing trend of CPP for increasing glottal insufficiencies reported in Fig. 6 (B) is consistent with [57, 46, 73, 74]. In accordance with [24, Fig. 12], where a distinction of VF motion asymmetries was not evident based on their evaluated features, the acoustic features of the present work also do not allow for the discrimination of VF motion asymmetry. Similar to [74, 24], we conclude that asymmetries in the VF motion are not necessarily related with a reduction in voice quality. The numerical range of our results is similar to the results of [24]. Furthermore, the subglottal pressure can be discriminated into two groups, i.e. 385 Pa and {775, 1500} Pa by using the features SPL, alpha ratio and HBI, mainly.

## 3.2 LDA/SVM Classification

In the following figures, the background is colored according to the class boundaries evaluated with SVM. The coloring of the data points indicates if the SVM is able to classify the point correctly: the inner dot represents the true class, and the outer ring represents the predicted class by SVM. From these figures, we see how the simulation configurations cluster in the dimension-reduced feature space. Furthermore, a graphical indication of class boundaries is provided. The class boundaries are obtained by classifying points of a mesh grid in the two-dimensional space with the trained SVM classifier.

**LDA & SVM for Glottal Closure Type** In Fig. 9, the result of the dimensionality reduction with LDA is visualized for all configurations using the pressure signal evaluated at the microphone point with respect to *glottal closure type*.

From Fig. 9, we see that a clear separation is possible between GC4 and {GC1, GC2, GC3}. The classes GC1, GC2, and GC3 are interwoven in the 2D-space. Thus, the training score<sup>2</sup> is only 75%. Misclassifications occur primarily for GC2 and GC3.

**LDA & SVM for Subglottal Pressure** In Fig. 10, the result of the dimensionality reduction with LDA is visualized for all configurations using the pressure signal evaluated at the microphone point with respect to *subglottal pressure*. In Fig. 10, it is visible that a good class separability is given for the three subglottal pressures, which is resembled in the training score of 91.7%. Especially the configurations with 775 Pa are well separated from the others.

**LDA & SVM for Symmetry** In Fig. 11, the result of the dimensionality reduction with LDA is visualized for the pressure signal evaluated at the microphone point with respect to the *symmetry* property. From

<sup>2</sup>The training score is obtained as follows. First the SVM is trained with all 24 configurations. Then the SVM is evaluated at the data points and the percentage of true classifications in relation to the total data is the training score.

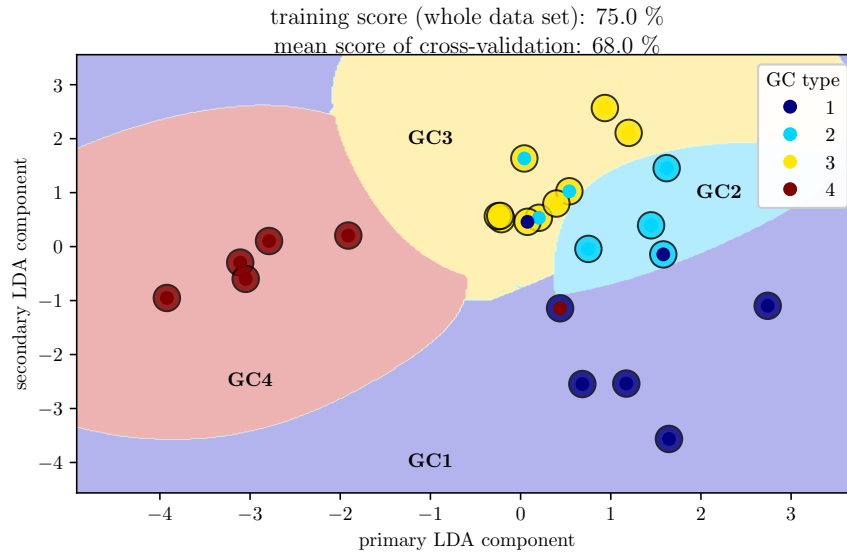


Figure 9: (color online) LDA-Reduced dimensionality of feature space and 2D-SVM classification of the glottal closure type for acoustic pressure signals at the microphone position. The points are colored according to the true GC type. The colored ring around each point denotes the predicted GC type. The background colors show the predicted GC types of the dimension-reduced feature space as labeled, and thus the class boundaries.

Fig. 11 we might conclude that a good class separability is given because the class boundary is clearly between two clusters. Still, there are many data samples located at the wrong side of the class boundary which is obvious from the training score of 70.8 %.

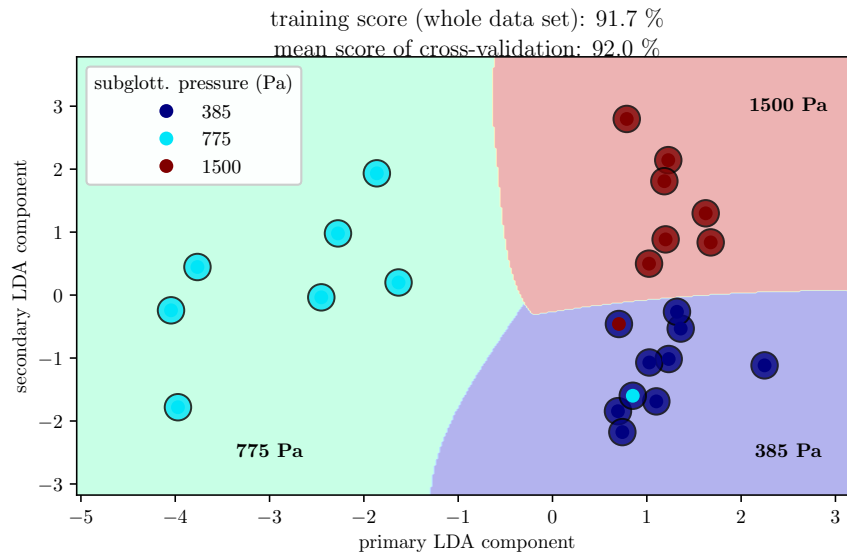


Figure 10: LDA-Reduced dimensionality of feature space and 2D-SVM classification of the subglottal pressure for acoustic pressure signals at the microphone position. The points are colored according to the true subglottal pressure. The colored ring around each point denotes the predicted subglottal pressure. The background colors show the predicted subglottal pressure class of the dimension-reduced feature space as labeled, and thus the class boundaries.

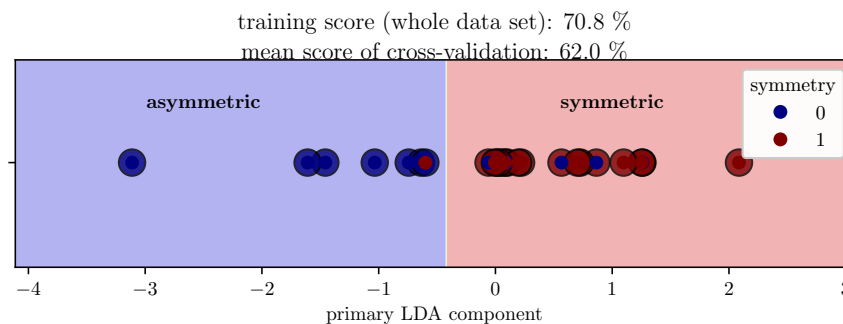


Figure 11: LDA-Reduced dimensionality of feature space and 2D-SVM classification of the symmetry for acoustic pressure signals at the microphone position. The points are colored according to the true symmetry class. The colored ring around each point denotes the predicted symmetry class. The background colors show the predicted symmetry class of the dimension-reduced feature space as labeled, and thus the class boundary.

## 4 Conclusion

Individuals affected by voice disorders have a significant reduction of their quality of life. Therefore, a simulation model *simVoice* was developed to investigate typical characteristics of voice such as sub-glottal pressure and of functional voice disorders as glottal closure insufficiency and left-right asymmetry. Based on 24 different voice configurations, we study voice parameters (HNR, CPP, ...) in the prospect of analyzing the flow-induced noise generation. Although multiple studies are based on experimental data, this is one of the first studies learning simulated data of healthy and disordered voice signals. A major limitation of our investigations is that the dataset is small, but the definition of relevant characteristics are precise and based on the *simVoice* model. Furthermore, the small dataset is analyzed by correlation analysis, and an SVM classifier with RBF kernel. With the use of LDA the dimensions of the individual representations are visualized in 2D. This allows to draw first correlations and determine the most important features evaluated from the acoustic signals in front of the mouth. Based on the definition of the acoustic features and with focus on the two lower formants, we found that a low-pass filtering with a cut-off frequency of 2 kHz provides a reasonable basis for further analysis. Regarding the results, conclusions can be drawn as follows. The GC type can be best discriminated based on CPP. The SPL allows discriminating subglottal pressure into two groups. The glottal symmetry does not have any effect on the evaluated features. Using the LDA-dimensionality-reduced feature space, one can best classify subglottal pressure with 91.7% accuracy. In addition to that the GC type can be classified with 75% accuracy. Finally, the symmetry property exhibits interwoven clusters and hence a classification is rather inaccurate.

## Acknowledgment

We acknowledge support from the Austrian Academy of Sciences (ÖAW), research grant "Understanding voice disorders", received from "Dr. Anton Oelzelt-Newin'sche Stiftung".

## References

- [1] I. R. Titze, Principles of Voice Production, 2nd Edition, National Center for Voice and Speech, 2000.
- [2] S. Schoder, M. Weitz, P. Maurerlehner, A. Hauser, S. Falk, S. Kniesburges, M. Döllinger, M. Kaltenbacher, Hybrid aeroacoustic approach for the efficient numerical simulation of human phonation, *J. Acoust. Soc. Am.* 147 (2) (2020) 1179–1194. doi:10.1121/10.0000785.
- [3] J. B. Park, L. Mongeau, Experimental investigation of the influence of a posterior gap on glottal flow and sound, *J. Acoust. Soc. Am.* 124 (2) (2008) 1171–1179. arXiv:https://doi.org/10.1121/1.2945116, doi:10.1121/1.2945116.
- [4] A. Yamauchi, H. Yokonishi, H. Imagawa, K.-I. Sakakibara, T. Nito, N. Tayama, T. Yamasoba, Age- and gender-related difference of vocal fold vibration and glottal configuration in normal speakers: Analysis with glottal area waveform, *J Voice* 28 (5) (2014) 525–531. doi:10.1016/j.jvoice.2014.01.016.
- [5] M. R. Hoffman, K. Surender, E. E. Devine, J. J. Jiang, Classification of glottic insufficiency and tension asymmetry using a multilayer perceptron, *Laryngoscope* 122 (12) (2012) 2773–2780. doi:10.1002/lary.23549.
- [6] L. A. Rammage, R. C. Peppard, D. M. Bless, Aerodynamic, laryngoscopic, and perceptual-acoustic characteristics in dysphonic females with posterior glottal chinks: A retrospective study, *J Voice* 6 (1) (1992) 64–78. doi:10.1016/S0892-1997(05)80010-4.
- [7] E. C. Inwald, M. Döllinger, M. Schuster, U. Eysholdt, C. Bohr, Multiparametric analysis of vocal fold vibrations in healthy and disordered voices in high-speed imaging, *J Voice* 25 (5) (2011) 576–590. doi:10.1016/j.jvoice.2010.04.004.
- [8] R. R. Patel, A. Dixon, A. Richmond, K. D. Donohue, Pediatric high speed digital imaging of vocal fold vibration: A normative pilot study of glottal closure and phase closure characteristics, *Int. J. Pediatr. Otorhinolaryngol.* 76 (7) (2012) 954–959. doi:10.1016/j.ijporl.2012.03.004.
- [9] B. Schneider, W. Bigenzahn, Influence of glottal closure configuration on vocal efficacy in young normal-speaking women, *J Voice* 17 (4) (2003) 468–480. doi:10.1067/S0892-1997(03)00065-1.
- [10] M. Vaca, I. Cobeta, E. Mora, P. Reyes, Clinical assessment of glottal insufficiency in age-related dysphonia, *J Voice* 31 (1) (2017) 128.e1–128.e5. doi:10.1016/j.jvoice.2015.12.010.
- [11] M. Södersten, S. Hertegård, B. Hammarberg, Glottal closure, transglottal airflow, and voice quality in healthy middle-aged women, *J Voice* 9 (2) (1995) 182–197. doi:10.1016/S0892-1997(05)80252-8.

- [12] S. Moccia, G. O. Vanone, E. De Momi, A. Laborai, L. Guastini, G. Peretti, L. S. Mattos, Learning-based classification of informative laryngoscopic frames, *Computer methods and programs in biomedicine* 158 (2018) 21–30.
- [13] H. Cordeiro, J. Fonseca, I. Guimarães, C. Meneses, Hierarchical classification and system combination for automatically identifying physiological and neuromuscular laryngeal pathologies, *Journal of voice* 31 (3) (2017) 384–e9.
- [14] M.-H. Laves, J. Bicker, L. A. Kahrs, T. Ortmaier, A dataset of laryngeal endoscopic images with comparative study on convolution neural network-based semantic segmentation, *International journal of computer assisted radiology and surgery* 14 (3) (2019) 483–492.
- [15] D. E. Callan, R. D. Kent, N. Roy, S. M. Tasko, Self-organizing map for the classification of normal and disordered female voices, *Journal of Speech, Language, and Hearing Research* 42 (2) (1999) 355–366.
- [16] S. N. Awan, N. Roy, Acoustic prediction of voice type in women with functional dysphonia, *Journal of voice* 19 (2) (2005) 268–282.
- [17] D. Voigt, M. Döllinger, T. Braunschweig, A. Yang, U. Eysholdt, J. Lohscheller, Classification of functional voice disorders based on phonovibrograms, *Artificial Intelligence in Medicine* 49 (1) (2010) 51–59.
- [18] D. Panek, A. Skalski, J. Gajda, R. Tadeusiewicz, Acoustic analysis assessment in speech pathology detection, *International Journal of Applied Mathematics and Computer Science* 25 (3) (2015) 631–643.
- [19] S. Umapathy, S. Rachel, R. Thulasi, Automated speech signal analysis based on feature extraction and classification of spasmodic dysphonia: a performance comparison of different classifiers, *International Journal of Speech Technology* 21 (1) (2018) 9–18.
- [20] A. Sama, P. Carding, S. Price, P. Kelly, J. Wilson, The clinical features of functional dysphonia, *The Laryngoscope* 111 (3) (2001) 458–463.
- [21] P. Schlegel, M. Stingl, M. Kunduk, S. Kniesburges, C. Bohr, M. Döllinger, Dependencies and ill-designed parameters within high-speed videoendoscopy and acoustic signal analysis, *Journal of Voice* 33 (5) (2019) 811–e1.
- [22] P. Schlegel, M. Kunduk, M. Stingl, M. Semmler, M. Döllinger, C. Bohr, A. Schützenberger, Influence of spatial camera resolution in high-speed videoendoscopy on laryngeal parameters, *PloS one* 14 (4) (2019) e0215168.
- [23] P. Schlegel, S. Kniesburges, S. Dürr, A. Schützenberger, M. Döllinger, Machine learning based identification of relevant parameters for functional voice disorders derived from endoscopic high-speed recordings, *scientific reports* 10 (1) (2020) 1–14.
- [24] S. Falk, S. Kniesburges, S. Schoder, B. Jakubaß, P. Maurerlehner, M. Echternach, M. Kaltenbacher, M. Döllinger, 3D-FV-FE aeroacoustic larynx model for investigation of functional based voice disorders, *Front. Physiol.* 12 (2021) 226. doi:10.3389/fphys.2021.616985.
- [25] S. Schoder, P. Maurerlehner, A. Wurzinger, A. Hauser, S. Falk, S. Kniesburges, M. Döllinger, M. Kaltenbacher, Aeroacoustic sound source characterization of the human voice production-perturbed convective wave equation, *Appl. Sci.* 11 (6). doi:10.3390/app11062614.
- [26] H. Sadeghi, M. Döllinger, M. Kaltenbacher, S. Kniesburges, Aerodynamic impact of the ventricular folds in computational larynx models, *J. Acoust. Soc. Am.* 145 (4) (2019) 2376–2387. doi:10.1121/1.5098775.
- [27] H. Sadeghi, S. Kniesburges, M. Kaltenbacher, A. Schützenberger, M. Döllinger, Computational models of laryngeal aerodynamics: Potentials and numerical costs, *J Voice* 33 (4) (2019) 385–400. doi:10.1016/j.jvoice.2018.01.001.
- [28] H. Sadeghi, S. Kniesburges, S. Falk, M. Kaltenbacher, A. Schützenberger, M. Döllinger, Towards a clinically applicable computational larynx model, *Appl. Sci.* 9 (11). doi:10.3390/app9112288.
- [29] P. Maurerlehner, S. Schoder, C. Freidhager, A. Wurzinger, A. Hauser, F. Kraxberger, S. Falk, S. Kniesburges, M. Echternach, M. Döllinger, M. Kaltenbacher, Efficient numerical simulation of the human voice, *e & i Elektrotechnik und Informationstechnik* 138 (3) (2021) 219–228. doi:10.1007/s00502-021-00886-1.
- [30] F. Alias, J. C. Socoro, X. Sevillano, A review of physical and perceptual feature extraction techniques for speech, music and environmental sounds, *Appl. Sci.* 6 (5). doi:10.3390/app6050143.
- [31] F. Eyben, *Real-time Speech and Music Classification by Large Audio Feature Space Extraction*, Springer Theses, Springer International, 2016. doi:10.1007/978-3-319-27299-3.
- [32] J. T. Geiger, B. Schuller, G. Rigoll, Large-scale audio feature extraction and svm for acoustic scene classification, in: *2013 IEEE Workshop on Applications of Signal Processing to Audio and Acoustics*, 2013, pp. 1–4. doi:10.1109/WASPAA.2013.6701857.

- [33] I. Mierswa, K. Morik, Automatic feature extraction for classifying audio data, *Mach. Learn.* 58 (2) (2005) 127–149. doi:10.1007/s10994-005-5824-7.
- [34] S. Schoder, F. Kraxberger, S. Falk, A. Wurzinger, K. Roppert, S. Kniesburges, M. Döllinger, M. Kaltenbacher, Error detection and filtering of incompressible flow simulations for aeroacoustic predictions of human voice, *J. Acoust. Soc. Am.* (under review).
- [35] M. Kaltenbacher, *Numerical Simulation of Mechatronic Sensors and Actuators: Finite Elements for Computational Multiphysics*, 3rd Edition, Springer, Berlin–Heidelberg, 2015. doi:10.1007/978-3-642-40170-1.
- [36] S. Schoder, K. Roppert, *opencfs: Open source finite element software for coupled field simulation–part acoustics*, arXiv preprint arXiv:2207.04443.
- [37] B. Kaltenbacher, M. Kaltenbacher, I. Sim, A modified and stable version of a perfectly matched layer technique for the 3-d second order wave equation in time domain with an application to aeroacoustics, *J. Comput. Phys.* 235 (2013) 407–422. doi:10.1016/j.jcp.2012.10.016.
- [38] J. Probst, A. Lodermeier, S. Fattoum, S. Becker, M. Echternach, B. Richter, M. Döllinger, S. Kniesburges, Acoustic and aerodynamic coupling during phonation in mri-based vocal tract replicas, *Appl. Sci.* 9 (17). doi:10.3390/app9173562.
- [39] S. Falk, *Numerical computation of functional voice disorders*, Ph.D. thesis, FAU Erlangen-Nürnberg (2021).
- [40] M. A. Belsky, S. D. Rothenberger, A. I. Gillespie, J. L. Gartner-Schmidt, Do phonatory aerodynamic and acoustic measures in connected speech differ between vocally healthy adults and patients diagnosed with muscle tension dysphonia?, *J Voice* 35 (4) (2021) 663.e1–663.e7. doi:10.1016/j.jvoice.2019.12.019.
- [41] O. Garaycochea, J. M. A. Navarrete, B. del Río, S. Fernández, Muscle tension dysphonia: Which laryngoscopic features can we rely on for diagnosis?, *J Voice* 33 (5) (2019) 812.e15–812.e18. doi:10.1016/j.jvoice.2018.04.015.
- [42] S. Kniesburges, A. Lodermeier, M. Semmler, Y. K. Schulz, A. Schützenberger, S. Becker, Analysis of the tonal sound generation during phonation with and without glottis closure, *J. Acoust. Soc. Am.* 147 (5) (2020) 3285–3293. doi:10.1121/10.0001184.
- [43] R. Patel, D. Dubrovskiy, M. Döllinger, Characterizing vibratory kinematics in children and adults with high-speed digital imaging, *J Speech Lang Hear Res* 57 (2) (2014) S674–S686. doi:10.1044/2014\_JSLHR-S-12-0278.
- [44] Z. Zhang, Compensation strategies in voice production with glottal insufficiency, *J Voice* 33 (1) (2019) 96–102. doi:10.1016/j.jvoice.2017.10.002.
- [45] A. Lodermeier, S. Becker, M. Döllinger, S. Kniesburges, Phase-locked flow field analysis in a synthetic human larynx model, *Exp. Fluids* 56 (4) (2015) 77. doi:10.1007/s00348-015-1942-6.
- [46] V. Birk, S. Kniesburges, M. Semmler, D. A. Berry, C. Bohr, M. Döllinger, A. Schützenberger, Influence of glottal closure on the phonatory process in ex vivo porcine larynges, *J. Acoust. Soc. Am.* 142 (4) (2017) 2197–2207. doi:10.1121/1.5007952.
- [47] P. Maurerlehner, *Efficient FEM model of human phonation*, Master’s thesis, TU Wien, Vienna (Mar. 2020).
- [48] P. Woo, A. K. Parasher, T. Isseroff, A. Richards, M. Sivak, Analysis of laryngoscopic features in patients with unilateral vocal fold paresis, *Laryngoscope* 126 (8) (2016) 1831–1836. doi:10.1002/lary.25790.
- [49] S. S. Azar, P. Pillutla, L. K. Evans, Z. Zhang, J. Kreiman, D. K. Chhetri, Perceptual evaluation of vocal fold vibratory asymmetry, *Laryngoscope* 131 (12) (2021) 2740–2746. doi:10.1002/lary.29679.
- [50] A. V. Oppenheim, J. R. Buck, R. W. Schaffer, *Discrete-Time Signal Processing*, 3rd Edition, Prentice-Hall signal processing series, Pearson Education, 2014. doi:10.5555/1795494.
- [51] E. Yumoto, W. J. Gould, T. Baer, Harmonics-to-noise ratio as an index of the degree of hoarseness, *J. Acoust. Soc. Am.* 71 (6) (1982) 1544–1550. doi:10.1121/1.387808.
- [52] K. Lee, C. Moon, Y. Nam, Diagnosing vocal disorders using cobweb clustering of the jitter, shimmer, and harmonics-to-noise ratio, *KSII T. Internet Info.* 12 (11) (2018) 5541–5554. doi:10.3837/tiis.2018.11.020.
- [53] J. Kreiman, B. R. Gerratt, M. Garellek, R. Samlan, Z. Zhang, Toward a unified theory of voice production and perception, *Loquens* 1 (27135054) (2014) e009. doi:10.3989/loquens.2014.009.
- [54] C. T. Ferrand, Harmonics-to-noise ratio: an index of vocal aging, *J Voice* 16 (2002) 480–7. doi:10.1016/s0892-1997(02)00123-6.
- [55] B. P. Bogert, M. J. R. Healy, J. W. Tukey, The quefrency analysis of time series for echoes: Cepstrum, pseudo-autocovariance, cross-cepstrum and saphe cracking, in: M. Rosenblatt (Ed.), *Proc. of the Symposium on Time Series Analysis*, John Wiley & Sons, Inc., New York, 1963, pp. 209–243.



- [56] J. Hillenbrand, R. A. Cleveland, R. L. Erickson, Acoustic correlates of breathy vocal quality, *J. Speech Hear.* 37 (1994) 769–778. doi:10.1044/jshr.3704.769.
- [57] J. Hillenbrand, R. A. Houde, Acoustic correlates of breathy vocal quality: dysphonic voices and continuous speech., *J. Speech Hear.* 39 (1996) 311–321. doi:10.1044/jshr.3902.311.
- [58] P. Welch, The use of fast fourier transform for the estimation of power spectra: A method based on time averaging over short, modified periodograms, *IEEE Trans. Audio Electroacoust.* 15 (2) (1967) 70–73. doi:10.1109/TAU.1967.1161901.
- [59] A. L. Rosenthal, S. Y. Lowell, R. H. Colton, Aerodynamic and acoustic features of vocal effort, *J Voice* 28 (2) (2014) 144–153. doi:10.1016/j.jvoice.2013.09.007.
- [60] Y. Maryn, P. Corthals, P. Van Cauwenberge, N. Roy, M. De Bodt, Toward improved ecological validity in the acoustic measurement of overall voice quality: Combining continuous speech and sustained vowels, *J Voice* 24 (5) (2010) 540–555. doi:10.1016/j.jvoice.2008.12.014.
- [61] Y. Maryn, M. De Bodt, N. Roy, The acoustic voice quality index: Toward improved treatment outcomes assessment in voice disorders, *J. Commun. Disord.* 43 (3) (2010) 161–174. doi:10.1016/j.jcomdis.2009.12.004.
- [62] Y. Maryn, N. Roy, M. De Bodt, P. Van Cauwenberge, P. Corthals, Acoustic measurement of overall voice quality: a meta-analysis., *J. Acoust. Soc. Am.* 126 (2009) 2619–34. doi:10.1121/1.3224706.
- [63] A. Behrman, D. Finan, *Speech and voice science*, 4th Edition, Plural Publishing, 2021.
- [64] D. P. W. Ellis, *An Introduction to Signal Processing for Speech*, 2nd Edition, Blackwell Handbooks in Linguistics, Wiley-Blackwell, 2010, pp. 757–780. doi:10.1002/9781444317251.ch20.
- [65] B. Gold, N. Morgan, D. Ellis, *Speech and Audio Signal Processing*, 2nd Edition, John Wiley & Sons, 2011. doi:10.1002/9781118142882.
- [66] J. Kreiman, Y.-L. Shue, G. Chen, M. Iseli, B. R. Gerratt, J. Neubauer, A. Alwan, Variability in the relationships among voice quality, harmonic amplitudes, open quotient, and glottal area waveform shape in sustained phonation, *J. Acoust. Soc. Am.* 132 (23039455) (2012) 2625–2632. doi:10.1121/1.4747007.
- [67] G. Chen, J. Kreiman, Y. Shue, A. Alwan, Acoustic correlates of glottal gaps, in: *Proc. INTERSPEECH 2011*, ISCA, Florence, Italy, 2011, pp. 2673–2676.
- [68] S. Kakouros, O. Räsänen, P. Alku, Comparison of spectral tilt measures for sentence prominence in speech—effects of dimensionality and adverse noise conditions, *Speech Commun.* 103 (2018) 11–26. doi:10.1016/j.specom.2018.08.002.
- [69] B. Hammarberg, B. Fritzell, J. Gaufin, J. Sundberg, L. Wedin, Perceptual and acoustic correlates of abnormal voice qualities, *Acta Otolaryngol.* 90 (1-6) (1980) 441–451. doi:10.3109/00016488009131746.
- [70] S. Patel, K. Scherer, J. Sundberg, E. Björkner, Acoustic markers of emotions based on voice physiology, in: *Proc. Speech Prosody*, Vol. 100865, ISCA, 2010.
- [71] C. M. Bishop, *Pattern Recognition and Machine Learning*, Information Science and Statistics, Springer, 2006. doi:10.5555/1162264.
- [72] F. Pedregosa, G. Varoquaux, A. Gramfort, V. Michel, B. Thirion, O. Grisel, M. Blondel, P. Prettenhofer, R. Weiss, V. Dubourg, J. Vanderplas, A. Passos, D. Cournapeau, M. Brucher, M. Perrot, E. Duchesnay, Scikit-learn: Machine learning in Python, *J Mach Learn Res* 12 (2011) 2825–2830. doi:10.5555/1953048.2078195.
- [73] F. Thornton, M. Döllinger, S. Kniesburges, D. Berry, C. Alexiou, A. Schützenberger, Impact of subharmonic and aperiodic laryngeal dynamics on the phonatory process analyzed in ex vivo rabbit models, *Appl. Sci.* 9 (9). doi:10.3390/app9091963.
- [74] Z. Zhang, J. Kreiman, B. R. Gerratt, M. Garellek, Acoustic and perceptual effects of changes in body layer stiffness in symmetric and asymmetric vocal fold models, *J. Acoust. Soc. Am.* 133 (1) (2013) 453–462. doi:10.1121/1.4770235.